Characterization of Flake Boron Nitride Prepared from the Low Temperature Combustion Synthesized Precursor and Its Application for Dye Adsorption

Jinglong Qu [1], Qun Li [2], Chang Luo [2], Jin Cheng [3] and Xinmei Hou [2],*

[1] Central Iron & Steel Research Institute, Beijing 100081, China; yafeng_chen2013@163.com
[2] Collaborative Innovation Center of Steel Technology, University of Science and Technology Beijing, Beijing 100083, China; liqun_ustb@foxmail.com (Q.L.); 18811343484@163.com (C.L.)
[3] School of Metallurgical and Ecological Engineering, University of Science and Technology Beijing, Beijing 100083, China; chengjin@ustb.edu.cn
* Correspondence: houxinmeiustb@ustb.edu.cn; Tel./Fax: +86-10-6233-2570

check for updates

Abstract: Flake boron nitride (BN) in large yield was successfully synthesized at low temperature from the combustion synthesized precursor. The precursor was prepared by a low-temperature (350 °C) combustion synthesis (LCS) method using nitric acid (HNO_3), urea ($CO(NH_2)_2$), boric acid (H_3BO_3), and glucose ($C_6H_{12}O_6 \cdot H_2O$) as starting materials. The precursor consists of B_2O_3 and amorphous carbon and the morphology is composed of blocks with average diameters of about 10 μm by statistical methods using SEM at different fields. Then BN was synthesized at 900 °C in NH_3 at a heating rate of 5 °C min^{-1}. The as-prepared BN possesses a flake morphology and high specific surface area up to 936 m^2 g^{-1}. It also has high density structural defects and abundant $-NH_2/-OH$ groups. The surface groups improve its water wettability and electronegativity, which contributes to the rapid and selective adsorption performance, especially towards the cationic dyes. When 4 mg of the sample was added into a 100 mL RhB solution with an initial concentration of 5 mg L^{-1}, 95% of the RhB was removed within 1 min and the adsorption capacity is 125 mg g^{-1}. Importantly, the sample can be regenerated by heating at 400 °C in air.

Keywords: flake BN; low temperature combustion synthesis; organic pollutions; selective adsorption

1. Introduction

Highly efficient cleaning of water resources from various contaminants is one of the major goals in environmental protection. Among these available approaches, adsorption has been found to be superior due to the advantages of efficient, economic, and easy operation [1–3]. Usually the adsorbents are selected based mainly on a physisorption mechanism due to the efficiency [4–6]. Therefore, such structural factors as density defects and micro/mesopores play an important role. In addition, the sustainable recyclability with simple regeneration treatment is another important factor for the adsorbent practical use [7,8]. Recently researchers have focused on the development of various nanoporous adsorbents based on their low density and high specific surface area [9], especially the high porous nanomaterials, such as hexagonal boron nitride (h-BN) because of its unique polarity of B–N bonds, numerous density defects, large specific surface area, excellent oxidation resistance, and good chemical inertness. Therefore, BN exhibits excellent adsorption properties for a wide range of oils, solvents, and dyes [10–12]. Various synthetic methods have already been adopted to prepare porous BN, such as carbothermal reduction nitridation [13], vapor deposition [14], direct combination of boron and nitrogen [15], and hard template-based methods [16], etc. In addition to these traditional methods, other methods were also developed to synthesize BN recently. For instance, Zhao et al.

developed a vesicant-assisted gas-foaming approach to fabricate vesicular structural 3D BN ceramic foams [5]. Lei et al. reported a synthesis process of porous BN nanosheets relying on a dynamic templating approach [17]. Zhang et al. developed a modified hot-press benzene-thermal method to synthesize BN nanocarpets [18]. Xue et al. used a simple template-free method to prepare BN foam-like porous monoliths [19]. All of the methods mainly focus on fabricating a porous structure. Recently, Li et al. reported a chemical activation method to change the surface property of BN for enhanced cationic dye removal performance [20]. This offers us a hint to improve the selective and effective adsorption performance of BN by combining the novel synthetic methods for porous materials with surface modification.

　　　Different types of adsorbents require different treatments for regeneration. The sustainable recyclability with simple regeneration treatment is another important factor for the adsorbent practical use [21,22]. Due to the excellent oxidation resistance and good chemical inertness, heating regeneration is feasible for BN adsorbents and the heating operation is simple only at 400 °C in a muffle furnace. Herein flake BN was prepared by combining the LCS and carbothermal reduction and nitridation methods. Its surface property was further modified during material synthesis without any post reaction.

2. Results and Discussion

2.1. Characterization of the Flake BN

　　　The structure characteristic of the precursor and product was firstly confirmed by the XRD pattern. From Figure 1a, it can be seen that the precursor consists of B_2O_3 and amorphous carbon. As for the obtained product after reaction in NH_3, two diffraction peaks, i.e., 2θ = 20°–30° and 40°–45° corresponding to the (002) and (100) facets of hexagonal BN (h-BN) (PDF34-421) appear [23]. The peaks of the product are broadened, indicating the product has poor crystallization. However, the poor crystallinity of the as-obtained flake BN still possesses good thermal stability in air up to 900 °C or so (Figure 1b), which is comparable to the reported results in the literature [24]. In addition, negligible mass change below 850 °C can be observed in TG curves, indicating the obtained product is in high purity. The FTIR spectra of the sample are shown in Figure 1c, two strong peaks at 1397 and 799 cm^{-1} should be attributed to v(B–N) and δ(B–N–B) modes of h-BN [25]. While the weak and broad peak at 3221 cm^{-1} comes from the –OH/–NH_2 groups, indicating the surface is modified.

　　　The chemical states of the product were investigated using XPS. Figure 2a shows that the sample surface consists of N, B, C, and O with binding energies of N1s, B1s, C1s, and O1s at 398.62, 190.78, 284.8, and 532.5 eV, respectively. Figure 2b–d shows typical B1s, N1s, and O1s spectra. The binding energy is calibrated with reference to the C1s energy (284.8 eV). The B1s spectra in Figure 2b are identified to be B–N peak at 190.78 eV, and B–O peak at approximately 192.05 eV which originates from the hydroxidation of some boron atoms at the surface of the sample. The B–OH signal is observed at a higher binding energy than the B–N signal owing to higher electronegativity of the hydroxide anion compared to that of nitrogen, and yet in a lower bonding energy than B=O in B_2O_3 (~193 eV) due to the lower oxidation state in B–OH. The N1s spectra are identified to be a B–N peak at 398.37 eV and a N–H peak at approximately 400.1 eV. N–H bonds are presumably needed for edge termination and reflecting the reductive ammonia atmosphere [26], which is in agreement with the FTIR results (Figure 1c). The O1s speak in Figure 2d at 532.8 eV is ascribed to the adsorbed O_2 or surface hydroxyl species [27].
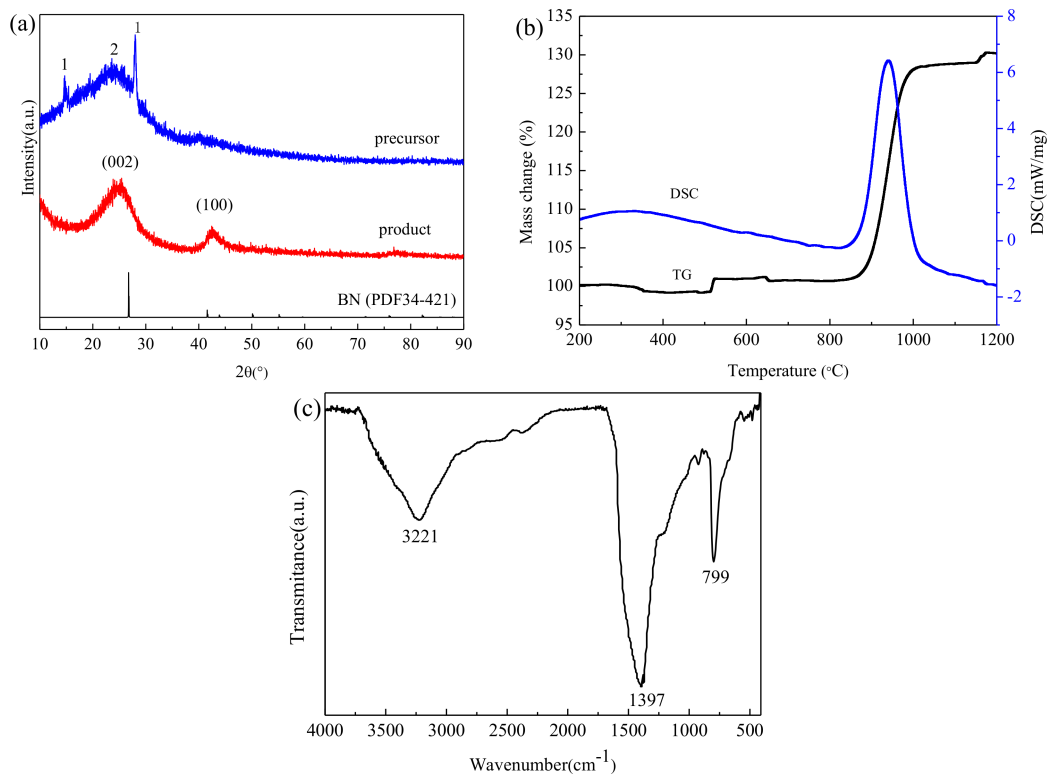
Figure 1. XRD pattern (**a**) of the precursor and the BN sample and the black vertical lines indicate the peak positions of the BN (PDF34-421) reflections. TG-DSC (**b**) and FIRT spectrum (**c**) of the BN.
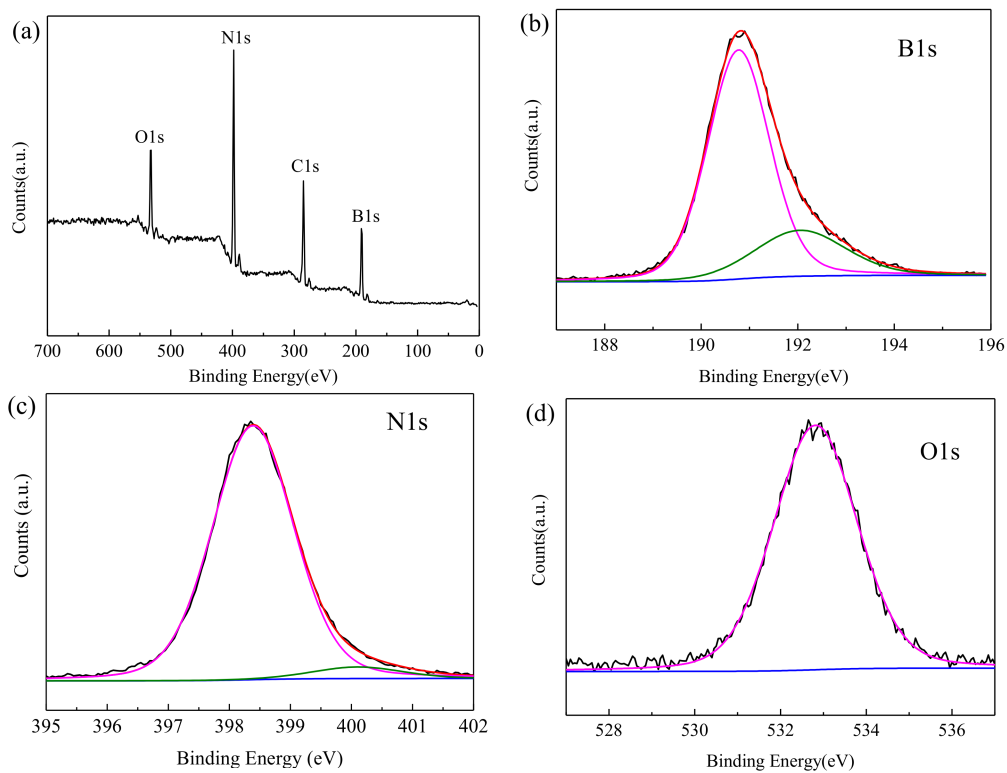
Figure 2. XPS spectra of the BN sample. (**a**) Survey spectrum; (**b**) B1*s*; (**c**) N1*s*; and (**d**) O1*s*.

The morphology of the precursor and h-BN product was characterized by SEM. Figure 3a shows the morphology of the precursor. It can be seen that the precursor consists of a large number of blocks with diameters of about 10 μm. Compared with the precursor, the morphology of the product becomes relatively thinner and changes into flake during atmosphere treatment as shown in Figure 3b,c. The surface microstructure of the obtained BN product is further investigated by TEM. As shown in the region marked by the black arrows in Figure 3d, the BN product possesses both rough surface and edge, indicating numerous surface defects exist in the flake BN. The HRTEM image in Figure 3e reveals five parallel fringes at the edge region of the flake and the interlayer distance is 0.357 nm, which is smaller than the standard value of h-BN (0.33–0.34 nm). The main reason is that the flake possesses a randomly stacked layer structure and amorphous structure as shown in Figure 3e. The corresponding SAED pattern (Figure 3f) shows two characteristic diffraction rings, which are indexed to the (110) and (101) planes of h-BN, respectively.
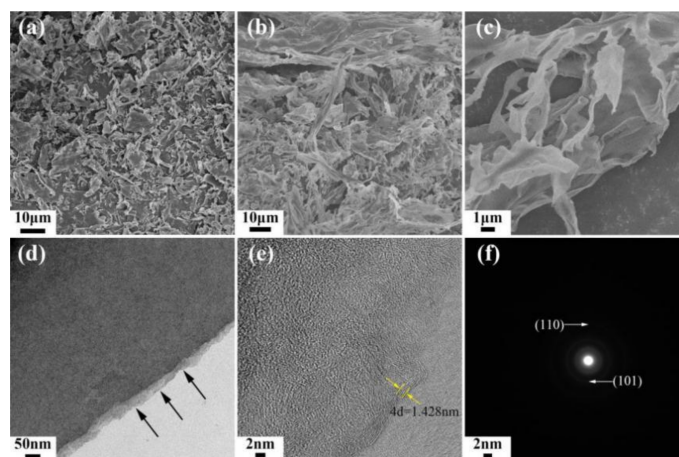

Figure 3. SEM images of the precursor (**a**) and the BN product (**b**,**c**); (**d**) TEM images of the BN product; (**e**) HRTEM; and (**f**) the SAED pattern.

The specific surface area of flake BN is determined by the nitrogen adsorption-desorption isotherm. As shown in Figure 4a, the isotherm can be classified as a type I isotherm with a type H4 hysteresis loop according to the IUPAC nomenclature [28], which indicates that the pores contain micropores and narrow slit-shaped mesopores. The specific surface area is calculated to be 936 m^2 g^{-1} according to the BET model. The total pore volume is 0.705 cm^3 g^{-1}. BJH calculations give a bimodal distribution with the main characteristic pore sizes of 2.2 and 3.4 nm (Figure 4b). Compared with the BN whiskers prepared in our recent work [29], the total pore volume of flake BN increases by 44%, which is beneficial in facilitating faster molecular diffusion to rapidly achieve the adsorption equilibrium [5].
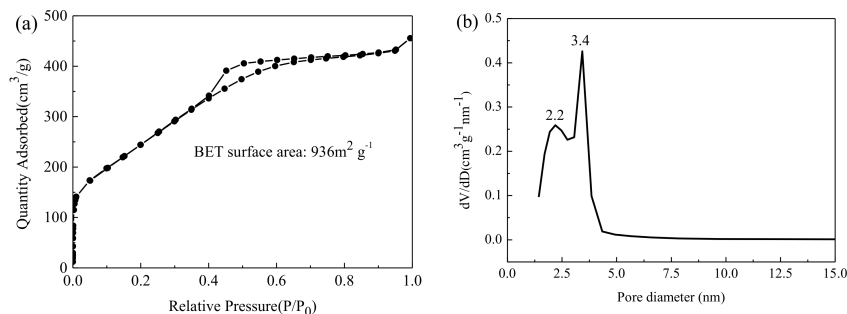

Figure 4. Nitrogen adsorption-desorption isotherm (**a**) and the corresponding pore size distribution of BN products (**b**).

2.2. Adsorption Performance of Flake BN

To demonstrate the potential applicability in wastewater treatment, we first chose rhodamine (RhB) as the indicant reagent to investigate the adsorption performance of the flake BN. The total adsorption and regeneration process is shown in Figure 5. As for the adsorption process, Figure 6a shows the UV–Vis adsorption spectroscopy of the RhB solution treated with flake BN at different time intervals at 553 nm. The inset of Figure 6a shows the corresponding photographic images of RhB solution taken at different times. As shown in Figure 6b, when 4 mg of the sample was added into a 100 mL RhB solution with an initial concentration of 5 mg L^{-1}, 95% of the RhB was removed within 1 min and only 5% was removed within the next 30 min at room temperature. Moreover, when the initial concentration of RhB increased from 5 to 25 mg L^{-1}, the removal percentage of RhB decreased from 99.3% to 56.7% (Figure 6c). Therefore, the removal efficiency of RhB decreases with an increase in the initial RhB concentration. The Langmuir models are widely employed to describe the relationship between the equilibrium adsorption capacity (q_e, mg g^{-1}) and its equilibrium solute concentration (C_e, mg L^{-1}) [30]:

$$q_e = \frac{q_m K_L C_e}{1 + K_L C_e} \tag{1}$$

where q_m is the maximum adsorption capacity of dyes (mg/g) corresponding to complete monolayer coverage and K_L is the equilibrium constant. Figure 6d shows that the Langmuir adsorption isotherm model fits the experimental data well with the correlation coefficients of 0.99. The Langmuir isotherm indicates that the maximum adsorption capacity is 359.71 mg g^{-1}, which is close to the maximum adsorption capacity of 354.35 mg g^{-1} with the initial concentration of 25 mg L^{-1} (Figure 6e). By comparison, the flake BN possesses higher or comparable adsorption capacity for RhB than previously reported results, including *Casuarina equisetifolia* needles (82.34 mg g^{-1}) [31], activated carbon (417.1 mg g^{-1}) [32], surface-modified tannery waste (213–250 mg g^{-1}) [33], *Azolla pinnata* (199.7 mg g^{-1}) [34], and three-dimensional foam-like h-BN (554 mg g^{-1}) [19].

Interestingly, the strong adsorption capacity was not obtained when the cationic dye RhB was changed to the anionic dye Congo red (CR). Figure 6f shows that only 36% of CR can be removed from water within 270 min at room temperature. The adsorption isotherm (Figure 6g) fitted by the Langmuir model gives a maximum adsorption capacity q_m of 70.9 mg g^{-1}, which is close to the maximum adsorption capacity of 64.2 mg g^{-1} with the initial concentration of 25 mg L^{-1} (Figure 6h). Compared with the adsorption capacity for RhB, the adsorption capacity for CR is relatively low. The results indicate that the flake BN can efficiently and selectively adsorb cationic dyes.
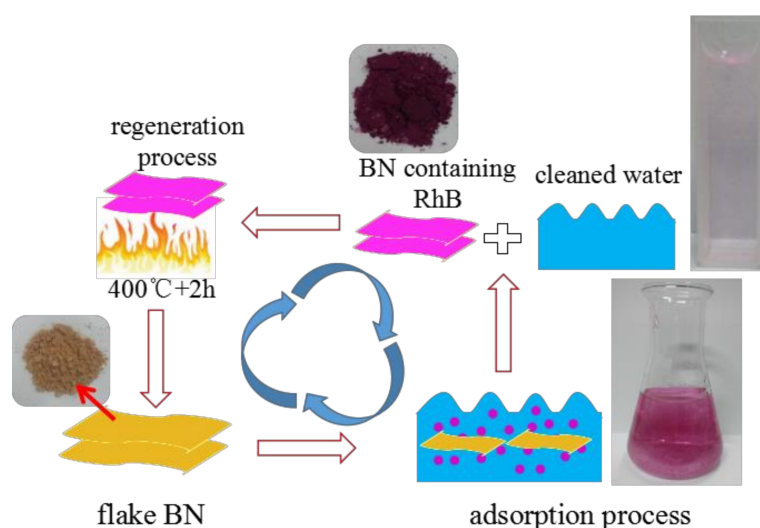

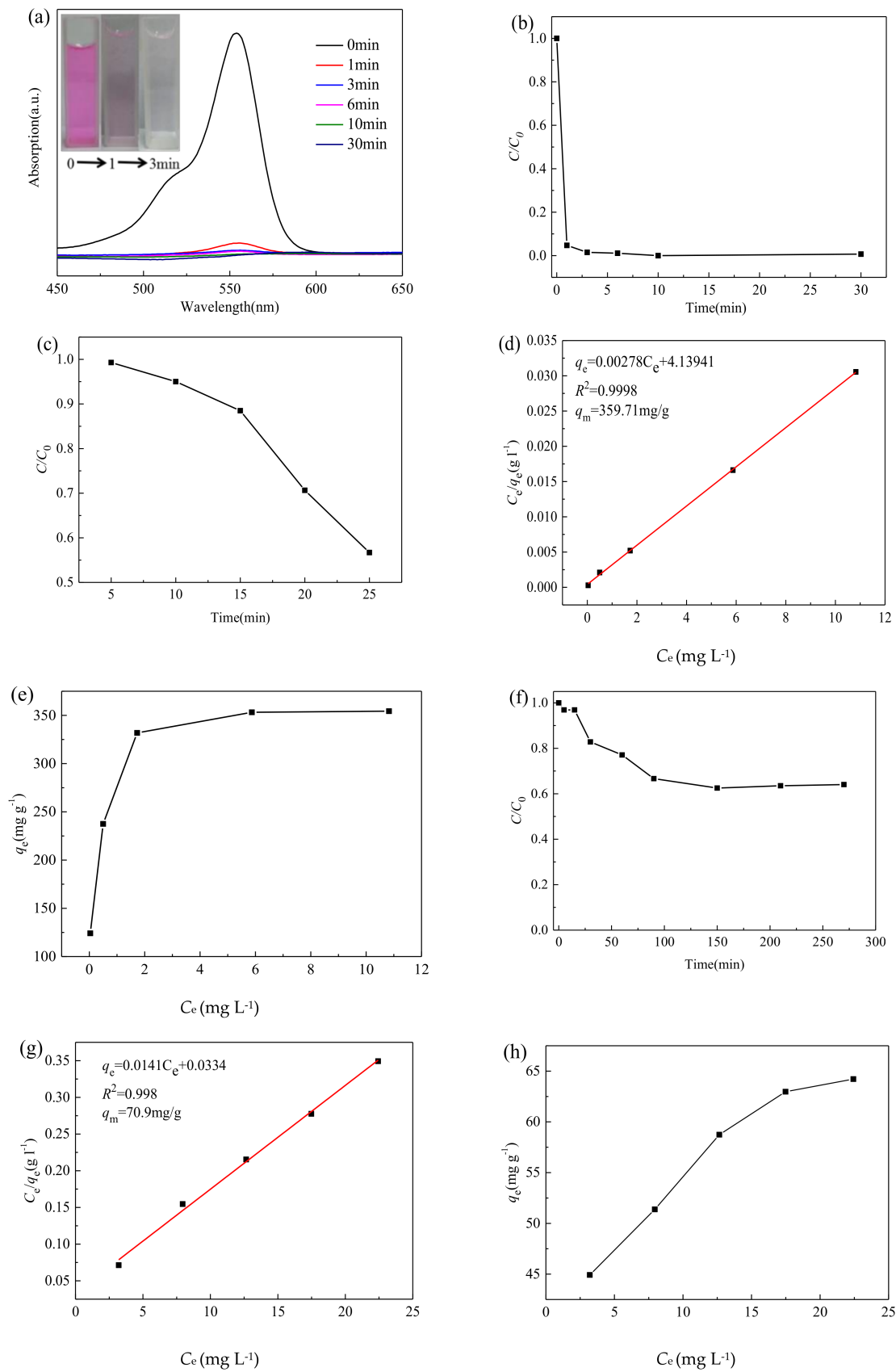**Figure 5.** The schematic of adsorption and regeneration process.
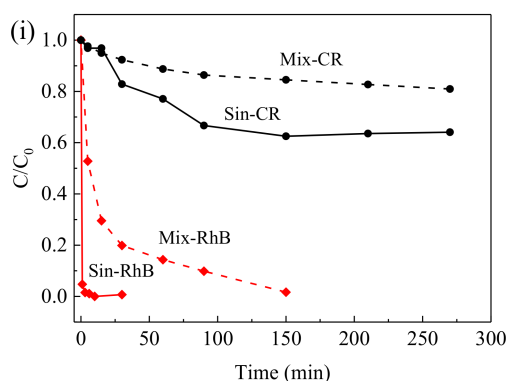
Figure 6. *Cont.*

Figure 6. (**a**) UV–Vis adsorption spectra and images (inset) of the aqueous RhB solution (5 mg L^{-1}, 100 mL) in the presence of the BN sample at different time interval; (**b**) Adsorption rates of RhB on the BN sample; (**c**) The percentage removal of RhB as a function of initial concentration; (**d**) the Langmuir isotherm and (**e**) the adsorption isotherm of RhB on the BN sample; (**f**) adsorption rates; (**g**) the Langmuir isotherm of CR on the BN sample; (**h**) the adsorption isotherm of CR on the BN sample; and (**i**) the removal rate of RhB (5 mg L^{-1}) and CR (10 mg L^{-1}) in single and mixed solution by adding 4 mg BN in 100 mL solution.

To further study the selectivity, the mixed solution including RhB and CR was used as shown in Figure 6e. From Figure 6e, it can be observed that the removal efficiency of RhB and CR decreases in the mixed solution when compared with the single RhB solution and CR solution, which is attributed to competitive adsorption between RhB and CR and active sites will be occupied by another dye. However, the removal rate of RhB still maintains 100% and the removal rate of CR decreases from 36% to 20%, which is due to the active groups and pore structure favored by RhB adsorption. This further demonstrates selectivity to some extent.

As for the efficiently selective adsorbed cationic dyes of flake BN, the reasons are following. Firstly, it is attributed to the surface active groups of the samples. The contact angle (CA) and zeta-potential of the obtained BN are also measured to explore its surface property. It is known that h-BN is naturally hydrophobic [15]. However, Figure 7a shows the sample obtained in our work is partially hydrophilic, which could result from the existence of –OH/–NH$_2$ groups [35]. Figure 7b shows that the sample has an overall negative surface charge at above pH 3.2. The low isoelectric point indicates that there are abundant acidic sites on the flake BN, which renders BN to be more suitable in the removal of cationic dyes from contaminated water systems [36]. Therefore, the abundant –OH on the surface of the flake BN changes the water wettability and electronegativity. This leads to a more negative charge and enhances the electrostatic attraction between the flake BN and cationic dye molecules. Additionally, the molecule size of CR (0.25 nm × 0.73 nm × 3 nm) [37] is larger than RhB (0.56 nm × 1.18 nm × 1.59 nm) [38] and can only enter into the above 3 nm pores. This limits the adsorption process between CR and the flake BN. Finally, the large surface area and non-covalent interaction, such as π-π stacking interaction between flake BN and aromatic rings, also make an important contribution to the adsorption capacity [39].
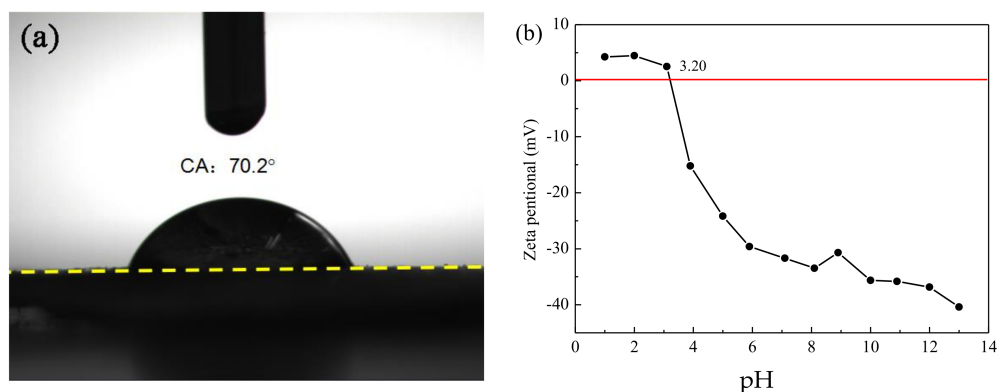
Figure 7. (**a**) CA and (**b**) Zeta potential vs. pH value of the flake BN.

As for the regeneration of the as-adsorbed flake BN, it is treated by a thermal route at 400 °C for 2 h in air. As shown in Figure 8, the reuse behavior was tested by adding 4 mg flake BN in 100 mL RhB (5 mg L^{-1}) for 10 cycles. The removal rate decreases by 20% after 10 cycles and the adsorption capacity decreases from 125 to 100 mg g^{-1} after 10 cycles, indicating the flake BN has high stability. To further avoid the decrease of removal rates, the high-temperature regeneration (400 °C) could be replaced in the future with more sustainable elution methods [40].
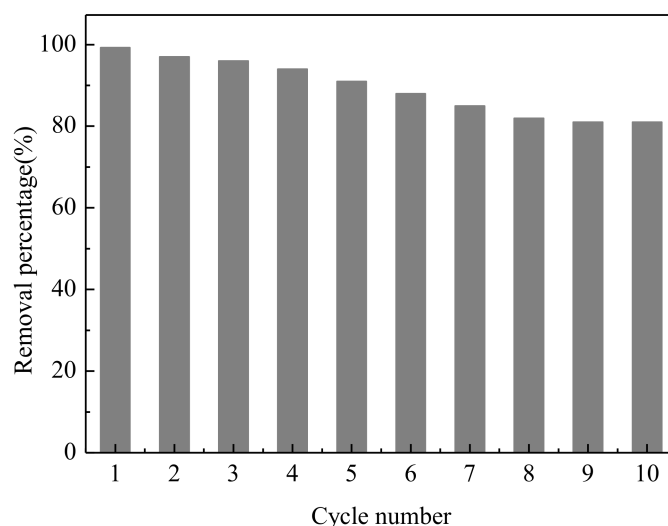

Figure 8. The removal percentage of RhB solution using recyclable BN sample within 10 times.

In addition, comparison of the SEM images and XRD patterns of flake BN before and after regeneration is shown in Figure 9. From Figure 9a–d, it can be seen that there is no obvious change for the morphology before Figure 9a,b and after Figure 9c,d regeneration, indicating that the structure of flake BN is stable and it can be used as an adsorbent. In addition, the XRD was used to investigate the phase of the flake BN before and after regeneration, as shown in Figure 9e. Compared with the flake BN, the peak at 2θ = 20°–30° slightly shift to large angle, which reveals the crystallization is improved. This is attributed to the reheating for regeneration, which will lead to reduce active sites for adsorption of dyes. Thus, the removal rate decreases by 20% after 10 cycles. Clearly, these results demonstrate that the obtained flake BN could be considered as a highly effective and recyclable adsorbent for the removal of pollutants in environment purification.
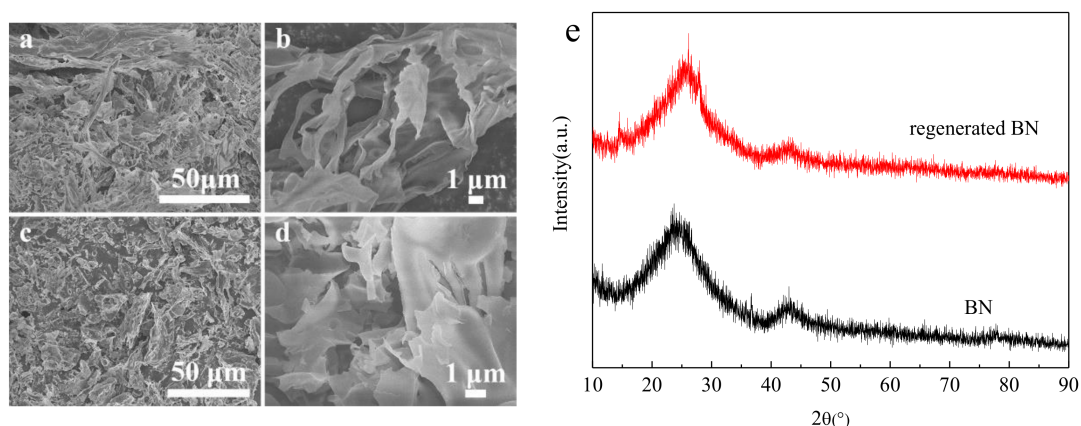
Figure 9. SEM images of the flake BN (**a**,**b**) and the regenerated flake BN after cycles (**c**,**d**); (**e**) XRD of the flake BN before and after regeneration.

3. Experimental Section

3.1. Chemicals and Reagents

H_3BO_3 (99.5 wt %), $C_6H_{12}O_6 \cdot H_2O$ (99.5 wt %), $CO(NH_2)_2$ (99.6 wt %) and HNO_3 (68 wt %) were of analytical grade and obtained from Beijing Chemical Co. Ltd. (Beijing, China); RhB ($C_{28}H_{31}ClN_2O_3$) and CR ($C_{32}H_{22}N_6Na_2O_6S_2$) were HPLC grade and purchased from Sigma-Aldrich Corporation (St. Louis, Missouri, USA). The pH was adjusted by 0.1 M NaOH (99 wt %) and 0.1 M HCl (35–37 wt %). Deionized water was used throughout the work. All chemicals were used without any further purification.

3.2. Preparation of BN

As shown in Figure 5, the preparation procedure includes two steps, i.e., (1) Synthesis of the precursor using H_3BO_3, $C_6H_{12}O_6 \cdot H_2O$, $CO(NH_2)_2$, and HNO_3 as raw materials via the LCS method. A transparent solution containing H_3BO_3, $C_6H_{12}O_6 \cdot H_2O$, $CO(NH_2)_2$ and HNO_3 with the mole ratio of 2:3:5:6 was filled into a crucible and heated to 350 °C in air in a muffle furnace at the heating rate of 15 °C min^{-1}. Initially the solution was boiling with increasing temperature. After a few minutes, the solution swelled suddenly, accompanying a release of large amount of gases. Then the furnace was turned off while the reaction continued for a few minutes. Finally, a fragile and foamy mixed precursor was obtained. (2) Conversion of the block precursor into flake BN at 900 °C in flowing NH_3. The obtained precursor was heated in a tube furnace at 900 °C for 3 h in flowing NH_3. Then the furnace was cooled naturally to room temperature in NH_3 and the yellow powder was obtained. The residual carbon was removed by firing at 600 °C in air for 2 h.

3.3. Characterization

The phases were identified by X-ray diffraction (XRD, M21XVHF22, MAC Science, Yokohama, Japan) with a TTRIII diffractometer equipped with Cu Kα radiation. The structure of the product was examined using Fourier transformation infrared spectroscopy (FTIR, Nicolet-Nexus 670, East Lyme, CT, USA) with spectral scanning between 4000 and 500 cm^{-1}. The thermogravimetric analysis was performed on a thermal analyzer (TG/DSC, Netzsch STA 449C, Selb, Bavaria, Germany). The chemical bonds of the product were determined by X-ray photoelectron spectra (XPS, AXISULTRA-DLD, Kratos, Manchester, UK) on an AXIS Ultra DLD X-ray photoelectron spectrometer using non-monochromatized Mg Kα X-rays as the excitation source. The surface morphology of the precursor and the product was observed by thermal field emission scanning electron microscopy (FE-SEM, ZEISS SUPRATM 55, Oberkochen, Germany) and transmission electron microscopy (TEM, HITACHI H8100, Hitachi,

Japan). High-resolution electron microscopy (HRTEM, JEM 2010, Joel Ltd., Tokyo, Japan) and selected area electron diffraction (SAED) patterns were used to characterize the phase and crystal morphology of the products. The specific surface area was determined from the nitrogen adsorption-desorption isotherm measured at 77K on a Quadrasorb SI-MP analyzer (Boynton beach, FL, USA) using the Brunauer-Emmett-Teller (BET) model. Contact angle (CA) was measured by the JC2000C4 contact angle goniometer (Powereach, Shanghai, China). UV–Vis spectra were recorded on a TU-1901 UV-visible spectrophotometer (Persee, Beijigng, China). Zeta potential values were recorded using a Zeta PALS, Brookhaven instrument (Suffolk, NY, USA), as a function of pH.

3.4. Water Treatment

Adsorption experiments were carried out by mixing BN (4 mg) with a dye solution (100 mL) in clean Erlenmeyer flasks and string at 200 rpm. RhB and CR, two kinds of dyes with opposite charges, are selected as the indicant reagents for measuring the adsorption performance of flake BN. The concentration of RhB and CR was examined at different time intervals by UV–Vis spectrophotometry at 553 and 497 nm, respectively. The equilibrium adsorption capacity q_e and adsorption rate E are calculated based on the concentration difference of RhB or CR in the aqueous solution before and after adsorption according to the following equation:

$$q_e = \frac{(C_0 - C_e)V}{m} \tag{2}$$

$$E = \frac{(C_0 - C_e)}{C_0} \times 100\% \tag{3}$$

where C_0 and C_e are the initial and equilibrium concentrations of dyes in solution (mg L^{-1}), V is the volume of solution (mL), m is the mass of adsorbent (mg). The concentration of dye solutions is determined after reference to the respective calibration curve of the dye using the Lambert-Beer law [41].

3.5. Regeneration

The regeneration of adsorbents is also critical to their practical application. The regeneration of flake BN was investigated by mixing BN (4 mg) with dye solution (100 mL) with stirring at 200 rpm, and then the as-adsorbed flake BN was heated and collected for the next use by a thermal route at 400 °C for 2 h in air.

4. Conclusions

Flake BN was fabricated using HNO_3, $CO(NH_2)_2$, H_3BO_3, and $C_6H_{12}O_6 \cdot H_2O$ as starting materials combining LCS, carbothermal reduction, and nitridiation methods. The obtained BN sample possesses a high surface area of 936 m^2 g^{-1} and is characterized as an amorphous and layered structure with high density defects and active surface groups. The adsorption processes for RhB and CR indicate that the flake BN exhibits an efficiently selective adsorption capacity for cationic dyes. It displays rapid adsorption performance for RhB and 95% of the RhB was removed within 1 min and the adsorption capacity is 125 mg g^{-1} with 100 mL RhB solution with an initial concentration of 5 mg L^{-1}. In addition, the sample can be easily regenerated at 400 °C in air and the adsorption capacity slightly decrease from 125 into 100 mg g^{-1} after 10 cycles. It can be expected that the flake BN will be a promising candidate for wastewater treatment.

Author Contributions: J.Q. and Q.L. contributed equally to this work. J.Q. and Q.L. performed the experiments and wrote the paper; C.L. helped to design the experiments and analyzed the data; X.H. revised the paper; and all five authors contributed to the discussion and conclusions.

Conflicts of Interest: The authors declare no conflict of interest.

References

1. Fan, L.; Luo, C.; Li, X.; Lu, F.; Qiu, H.; Sun, M. Fabrication of novel magnetic chitosan grafted with graphene oxide to enhance adsorption properties for methyl blue. *J. Hazard. Mater.* **2012**, *215*, 272–279. [CrossRef] [PubMed]

2. Guo, J.Z.; Li, B.; Liu, L.; Lv, K. Removal of methylene blue from aqueous solutions by chemically modified bamboo. *Chemosphere* **2014**, *111*, 225–231. [CrossRef] [PubMed]

3. Zhang, F.; Zhao, Z.; Tan, R. Selective and effective adsorption of methyl blue by barium phosphate nano-flake. *J. Colloid Interface Sci.* **2012**, *386*, 277–284. [CrossRef] [PubMed]

4. Li, J.; Lin, J.; Xu, X. Porous boron nitride with a high surface area: Hydrogen storage and water treatment. *Nanotechnology* **2013**, *24*, 155603. [CrossRef] [PubMed]

5. Zhao, H.; Song, X.; Zeng, H. 3D white graphene foam scavengers: Vesicant-assisted foaming boosts the gram-level yield and forms hierarchical pores for superstrong pollutant removal applications. *NPG Asia Mater.* **2015**, *7*, e168. [CrossRef]

6. Bhatnagar, A.; Jain, A.K. A comparative adsorption study with different industrial wastes as adsorbents for the removal of cationic dyes from water. *J. Colloid Interface Sci.* **2005**, *281*, 49–55. [CrossRef] [PubMed]

7. Razali, M.; Kim, J.F.; Attfield, M.; Budd, P.M.; Drioli, E.; Lee, Y.M.; Szekely, G. Sustainable wastewater treatment and recycling in membrane manufacturing. *Green Chem.* **2015**, *17*, 5196–5205. [CrossRef]

8. Qin, K.; Li, F.; Xu, S.; Wang, T.; Liu, C. Sequential removal of phosphate and cesium by using zirconium oxide: A demonstration of designing sustainable adsorbents for green water treatment. *Chem. Eng. J.* **2017**, *322*, 275–280. [CrossRef]

9. Ganji, M.D.; Mirnejad, A.; Najafi, A. Theoretical investigation of methane adsorption onto boron nitride and carbon nanotubes. *Sci. Technol. Adv. Mater.* **2010**, *11*, 045001. [CrossRef] [PubMed]

10. Li, J.; Jia, H.; Lin, J. Free-standing membranes made of activated boron nitride for efficient water cleaning. *RSC Adv.* **2015**, *5*, 71537–71543. [CrossRef]

11. Lvova, N.A.; Ananina, O.Y. Theoretical study of the adsorption properties of porous boron nitride nanosheets. *Comput. Mater. Sci.* **2016**, *115*, 11–17. [CrossRef]

12. Li, J.; Xiao, X.; Xu, X. Activated boron nitride as an effective adsorbent for metal ions and organic pollutants. *Sci. Rep.* **2013**, *3*, 3208. [CrossRef] [PubMed]

13. Hou, X.; Yu, Z.; Chou, K.C. Facile synthesis of hexagonal boron nitride fibers with uniform morphology. *Ceram. Int.* **2013**, *39*, 6427–6431. [CrossRef]

14. Pakdel, A.; Zhi, C.; Bando, Y.; Nakayama, T.; Golberg, D. A comprehensive analysis of the CVD growth of boron nitride nanotubes. *Nanotechnology* **2012**, *23*, 215601. [CrossRef] [PubMed]

15. Zhao, L.; Zhang, Y.J.; Gong, H.Y. Preparation and characterisation of boron nitride whiskers. *Mater. Res. Innov.* **2010**, *14*, 189–191. [CrossRef]

16. Dibandjo, P.; Chassagneux, F.; Bois, L.; Sigala, C.; Miele, P. Comparison between SBA-15 silica and CMK-3 carbon nanocasting for mesoporous boron nitride synthesis. *J. Mater. Chem.* **2005**, *15*, 1917–1923. [CrossRef]

17. Lei, W.; Portehault, D.; Liu, D.; Qin, S.; Chen, Y. Porous boron nitride nanosheets for effective water cleaning. *Nat. Commun.* **2013**, *4*, 1777. [CrossRef] [PubMed]

18. Zhang, X.; Lian, G.; Zhang, S.; Cui, D.; Wang, Q. Boron nitride nanocarpets: Controllable synthesis and their adsorption performance to organic pollutants. *CrystEngComm* **2012**, *14*, 4670–4676. [CrossRef]

19. Xue, Y.; Dai, P.; Jiang, X. Template-free synthesis of boron nitride foam-like porous monoliths and their high-end applications in water purification. *J. Mater. Chem. A* **2016**, *4*, 1469–1478. [CrossRef]

20. Li, J.; Huang, Y.; Liu, Z. Chemical activation of boron nitride fibers for improved cationic dye removal performance. *J. Mater. Chem. A* **2015**, *3*, 8185–8193. [CrossRef]

21. Shah, I.K.; Pre, P.; Alappat, B.J. Steam regeneration of adsorbents: An experimental and technical review. *Chem. Sci. Trans.* **2013**, *2*, 1078–1088.

22. Wang, S.; Li, H.; Xie, S.; Liu, S.; Xu, L. Physical and chemical regeneration of zeolitic adsorbents for dye removal in wastewater treatment. *Chemosphere* **2006**, *65*, 82–87. [CrossRef] [PubMed]

23. Hou, X.; Yu, Z.; Li, Y.; Chou, K.C. Preparation and properties of hexagonal boron nitride fibers used as high temperature membrane filter. *Mater. Res. Bull.* **2014**, *49*, 39–43. [CrossRef]

24. Zhu, H.L.; Han, Q.X.; Wu, J.; Meng, X.L.; Cui, H.Z. Large scale synthesis of nanoporous BN flake with high surface areas. *J. Cryst. Growth* **2016**, *434*, 19–24. [CrossRef]

25. Zheng, M.; Gu, Y.; Xu, Z.; Liu, Y. Synthesis and characterization of boron nitride nanoropes. *Mater. Lett.* **2007**, *61*, 1943–1945. [CrossRef]

26. Pakdel, A.; Bando, Y.; Golberg, D. Plasma-assisted interface engineering of boron nitride nanostructure films. *ACS Nano* **2014**, *8*, 10631–10639. [CrossRef] [PubMed]

27. Li, P.; Zhao, X.; Jia, C.J.; Sun, H.; Sun, L.; Cheng, X.; Liu, L.; Fan, W. ZnWO$_4$/BiOI heterostructures with highly efficient visible light photocatalytic activity: The case of interface lattice and energy level match. *J. Mater. Chem. A* **2013**, *1*, 3421–3429. [CrossRef]

28. Weng, Q.; Wang, X.; Zhi, C.; Bando, Y.; Golberg, D. Boron nitride porous microbelts for hydrogen storage. *ACS Nano* **2013**, *7*, 1558–1565. [CrossRef] [PubMed]

29. Li, Q.; Yang, T.; Yang, Q.; Wang, F.; Chou, K.C.; Hou, X. Porous hexagonal boron nitride whiskers fabricated at low temperature for effective removal of organic pollutants from water. *Ceram. Int.* **2016**, *42*, 8754–8762. [CrossRef]

30. Kannan, N.; Sundaram, M.M. Kinetics and mechanism of removal of methylene blue by adsorption on various carbons-a comparative study. *Dyes Pigment.* **2001**, *51*, 25–40. [CrossRef]

31. Kooh, M.R.R.; Dahri, M.K.; Lim, L.B. The removal of Rhodamine B dye from aqueous solution using *Casuarina equisetifolia* needles as adsorbent. *Cogent Environ. Sci.* **2016**, *2*, 1140553. [CrossRef]

32. Guo, Z.; Zhang, J.; Liu, H. Ultra-high Rhodamine B adsorption capacities from an aqueous solution by activated carbon derived from *Phragmites australis* doped with organic acid by phosphoric acid activation. *RSC Adv.* **2016**, *6*, 40818–40827. [CrossRef]

33. Anandkumar, J.; Mandal, B. Adsorption of chromium (VI) and Rhodamine B by surface modified tannery waste: Kinetic, mechanistic and thermodynamic studies. *J. Hazard. Mater.* **2011**, *186*, 1088–1096. [CrossRef] [PubMed]

34. Kooh, M.R.R.; Lim, L.B.; Lim, L.H.; Dahri, M.K. Separation of toxic Rhodamine B from aqueous solution using an efficient low-cost material, *Azolla pinnata*, by adsorption method. *Environ. Monit. Assess.* **2016**, *188*, 108. [CrossRef] [PubMed]

35. Lian, G.; Zhang, X.; Si, H.; Wang, J.; Cui, D.; Wang, Q. Boron nitride ultrathin fibrous nanonets: One-step synthesis and applications for ultrafast adsorption for water treatment and selective filtration of nanoparticles. *ACS Appl. Mater. Interface* **2013**, *5*, 12773–12778. [CrossRef] [PubMed]

36. Postai, D.L.; Demarchi, C.A.; Zanatta, F.; Melo, D.C.C.; Rodrigues, C.A. Adsorption of Rhodamine B and methylene blue dyes using waste of seeds of *Aleurites moluccana*, a low cost adsorbent. *Alex. Eng. J.* **2016**, *55*, 1713–1723. [CrossRef]

37. Zhang, Y.J.; Liu, L.C.; Ni, L.L.; Wang, B.L. A facile and low-cost synthesis of granulated blast furnace slag-based cementitious material coupled with Fe$_2$O$_3$ catalyst for treatment of dye wastewater. *Appl. Catal. B Environ.* **2013**, *138*, 9–16. [CrossRef]

38. Shen, J.; Wu, Y.N.; Zhang, B.; Li, F. Adsorption of Rhodamine B dye by biomimetic mesoporous SiO$_2$ nanosheets. *Clean Technol. Environ.* **2015**, *17*, 2289–2298. [CrossRef]

39. Xue, L.; Lu, B.; Wu, Z.S.; Ge, C.; Wang, P.; Zhang, R.; Zhang, X.D. Synthesis of mesoporous hexagonal boron nitride fibers with high surface area for efficient removal of organic pollutants. *Chem. Eng. J.* **2014**, *243*, 494–499. [CrossRef]

40. Kupai, J.; Razali, M.; Buyuktiryaki, S.; Kecili, R.; Szekely, G. Long-term stability and reusability of molecularly imprinted polymers. *Polym. Chem.* **2017**, *8*, 666–673. [CrossRef] [PubMed]

41. Nagia, F.A.; El-Mohamedy, R.S.R. Dyeing of wool with natural anthraquinone dyes from *Fusarium oxysporum*. *Dyes Pigment* **2007**, *75*, 550–555. [CrossRef]